METAL OXIDE HETEROSTRUCTURE BASED PHOTOCATALYSTS FOR ENVIRONMENT REMEDIAL APPLICATIONS

Abstract

The quest for sustainable solutions to address environmental challenges has led to significant research efforts in the development of advanced photocatalytic materials. Among these, metal oxide heterostructures have emerged as a promising class of materials with exceptional photocatalytic properties for environmental remediation applications. This article explores the recent advancements in the design, synthesis, and characterization of ZnO based metal oxide heterostructure-based photocatalysts, focusing on their applications in addressing environmental issues such as water and air pollution. In the present work, photocatalytic property of nanocomposites (NCs) of the metal oxides such as; ZnO and SnO_2 has been discussed by synthesizing the samples by using the sol-gel method. By using X-ray diffraction (XRD) analysis, the structural parameters have been determined and the formation of two phased composite having tetragonal phases of rutile (SnO_2) and wurtzite (ZnO) structures has been confirmed. FESEM study has been used to investigate the morphology along with the shape and surface property. The band gap of NC is higher than the band gaps of the individual oxides, according to optical absorbance investigation. Photocatalytic measurement shows improved degradation efficiency of the composites as compared to pristine samples. Prevention of rapid carrier recombination and the production of extremely reactive OH• and O_2•- radicals are accountable for the breakdown of toxic substances like phenol and Rhodamine B(RB). This happens due to the hoarded electrons and holes on SnO_2 and ZnO surfaces respectively. The photocatalytic mechanism has been explained thoroughly and after several iterations of experimentation, it was found that the nanocatalysts are incredibly stable and reusable.

Keywords: Nanocomposite, phenol, Rhodamine B, Photocatalyst, Tetragonal Rutile

Author

Dojalisa Sahu
School of Applied Sciences
Centurion University of Technology and Management
Odisha, India.

I. INTRODUCTION

Metal oxide heterostructure-based photocatalysts have the potential to be used in future sustainable technologies and their role in mitigating environmental pollution is widely discussed underscoring the importance of continued research and development in this field. As we confront pressing environmental challenges, the promising features of metal oxide heterostructure photocatalysts have evolved as a cornerstone in the quest for effective and eco-friendly solutions to remediate polluted ecosystems. In the context of environmental remediation, the application of metal oxide heterostructure photocatalysts for the degradation of organic pollutants, disinfection of water, and removal of harmful gases is comprehensively studied. Nanomaterials have unique properties which find several applications in different areas of technology. The field of nanotechnology has brought significant advancements in several disciplines by its ability to manipulate and engineer materials at the nanoscale [1-4]. Semiconducting nanoparticles have a significant position among the vast array of nanomaterials, owing to their distinct characteristics and extensive scope of utilization [5-8]. These materials demonstrate exceptional electrical, optical, and chemical characteristics, rendering them crucial foundational components for forthcoming technologies [9-14]. The size-dependent behaviour is a characteristic that distinguishes semiconducting nanomaterials. When a material is lowered to the nanoscale, the prominence of quantum confinement effects is observed [11-18]. Semiconducting nanomaterials possess the advantageous characteristic of adjustable bandgaps, hence enabling researchers to tailor materials according to specific applications [19-25]. The aforementioned feature plays a crucial role in the design of sensors, solar cells, and light-emitting devices. Nanomaterials exhibit a notable surface-to-volume ratio, rendering them highly suitable for a diverse range of catalytic and sensing applications [1-20]. The heightened surface area of the material facilitates enhanced interactions with other substances, hence resulting in enhanced performance in chemical reactions and the detection of analytes [21-28]. In addition to this, semiconducting nanomaterials demonstrate augmented optical characteristics as a result of their diminutive dimensions and quantum phenomena. These characteristics encompass robust absorption, elevated photoluminescence efficacy, and enhanced light scattering, rendering them well-suited for various applications such as light-emitting diodes (LEDs), lasers, and photodetectors [20-30]. Semiconducting nanomaterials are of utmost importance in contemporary electronics, as evidenced by a substantial body of research. Transistors, diodes, and memory devices incorporate them inside their structures. The higher charge transport capabilities of nanoscale transistors contribute to improved performance, leading to speedier and more energy-efficient electronic devices. Nanomaterials are utilized as photocatalysts to facilitate chemical processes through the utilization of light energy [13, 16-18]. These reactions have various applications, including their use in the process of water splitting for the production of hydrogen fuel, degradation of pollutants, and reduction of CO_2 [31-35]. The materials possess a significant surface area and adjustable bandgaps, which contribute to the improvement of their catalytic efficacy. Semiconducting nanoparticles are utilized in the context of environmental remediation procedures. Photocatalytic processes fuelled by solar energy enable the degradation of organic contaminants and the detoxification of water. The potential of this application to bring about a revolution in wastewater treatment and pollution elimination is significant [36-40]. Metal oxide semiconductors are materials that have received considerable interest owing to their wide array of characteristics and flexible uses. These materials possess distinctive electrical, optical, and chemical properties, rendering them indispensable for a wide range of technological breakthroughs. Metal oxide semiconductors (MOS) are a class

of materials that exhibit notable characteristics such as elevated electron mobility, gas sensing capabilities, photoresponse, catalytic properties, and thermal stability [18-28]. In the present course, zinc oxide (ZnO) and tin oxide (SnO_2) are regarded as functional materials that possess significant properties in the fields of optoelectronics, sensing, photocatalysis, and antibacterial efficacy [27-31]. Extensive research has been conducted on the photocatalytic characteristics of these materials, with numerous studies documenting their efficacy in the photodegradation of hazardous contaminants [16-18]. Zinc oxide (ZnO) is characterized by a notable energy difference between its valence and conduction bands, commonly referred to as the band gap (Eg), which measures 3.37 electron volts (eV). At ambient conditions, ZnO demonstrates absorption properties in the near-ultraviolet (UV) to deep violet range [2-25].

New semiconducting metal oxides such as TiO_2, ZnO and SnO_2 are lauded for their ability to emit light in the ultraviolet (UV) and visible spectrums. The PL characteristics of the oxide particles mentioned above are frequently modified by manipulating the Eg(band gap energy) through the addition of impurities. Similar observation can also be seen by coupling of two or more metal oxide, resulting in heteromolecular stucture that have a considerable impact on the carrier transportation procedure [41]. These transporters efficiently participate in various transitions under the impact of light with the appropriate energy, leading to PL emission which are unconventional in nature. The aforementioned materials are effective photocatalyzed substance for the complete breakdown of toxic pollutants into smaller components like CO_2 and H_2O, that are safe for bio-organisms [42-45]. They are chemically stable, less expensive, and non-toxic in nature. ZnO has unique properties like high excitonic binding energy (60 meV), wide band gap (3.37 eV), high carrier mobility, and additional surface reactivity [46]. A distinct UV emission along with visible defect-induced emission band are evident in the luminescence spectra of ZnO. In comparison to TiO_2, it has also greater visible light photocatalytic ability for reducing hazardous contaminant. Strong oxidizers such hydroxyl (OH•) radicals are produced when UV-Vis light fall on the ZnO catalytic surface. Numerous studies on heterostructure nanocomposites have been published in the literature, like formation of the combined heterostructure [25-30]. Tin oxide (SnO_2) is regarded as a multipurpose n-type semiconducting material with wide applications in the fields of Li batteries, solar cells, sensors, and photocatalysis [12, 13,24]. It has a strong excitonic binding energy of 130 meV and a wide band gap of 3.6 eV. SnO_2 exhibits a broad PL emission band with an oxygen vacancy-induced energy about 2 eV. Tin oxide's PL properties are highly responsive to variations in the optical band gap and can be enhanced by impurity doping, for example. Since tin oxide's conduction band edge is considerably large positive site that of TiO_2 and zinc oxide, it is considered as a better electron acceptor [13]. As a result, it is an ideal choice to join ZnO to create nanocomposites. The hybrid system is expected to have improved PC properties, which is most likely caused by the heterostructure's high charge separation efficiency [12]. Both the oxides, ZnO and SnO_2, are extensively explored as a result of their above-mentioned intriguing features. However, a good mechanism for the structural behaviour with light emission phenomenon of the aforementioned composite with different molar ratio has not been reported in detail. Similar to this, little is known about the photocatalytic effectiveness of ZnO and SnO_2 nanocomposite in the breakdown of dangerous organic pollutants such phenol(Ph) and Rhodamine B(RB). So this study might help in predicting the electronic structure along with photocatalytic proficiencies of ZnO and SnO_2 composite with appropriate methodology.

II. EXPERIMENTAL METHOD

1. **Synthesis of Photocatalyst:** The synthesis of ZnO, SnO_2, and ZnO/SnO_2 samples was done using the sol-gel method. As starting reagents, tin chloride ($SnCl_2.2H_2O$), ammonium hydroxide (NH_4OH), isopropyl alcohol, and zinc acetate dihydrate ($Zn(OAc)_2$) were used. phenol and Rhodamine B were two organic contaminants that were considered to be suitable for degradation by these particular photocatalysts. By dissolving $SnCl_2.2H_2O$ and $Zn(OAc)_2$ in ratio of 2:1 in double-distilled water (20 ml) and stirring continuously, the composite of ZnO/SnO_2 (1:0.5) was created. After vigorously whirling the above solution for 10 minutes, isopropyl alcohol (25 ml) was added to get a sol After another 15 minutes of stirring, the ammonia solution was added to the above reaction mixture. The solution was stirred for an additional 4 hours, after which the sample washed out using solvent and DD water. The obtained powdes were calcined again for two hours at 600 °C after being dried in the oven for eight hours at 120 °C. Using the same method, we created $ZnO:SnO_2$ nanocomposites with various concentrations (1:1 and 2:1), which we labelled ZS1 and ZS2, respectively.

2. **Photocatalytic Experiment:** The degradation of phenol and Rhodamine B under UV-Vis light irradiation was examined to determine the produced material's photo catalytic activity. Utilizing a photo-reactor with a visible light source, phenol and Rhodamine B degradation was carried out. The original concentration of the toxic chemicals (C_0) was 10 mg/L, the catalyst concentration was held at 5 mg/L. pH of the solution was noted as 6.5. Catalyst amount was varied from 5 to 25 mg/L, and initial toxic amount from 5 to 20 mg/L. The catalyst -pollutant solution was left in the dark for 30 minutes to achieve the adsorption/desorption equilibrium. The catalyst -pollutant solution was then exposed to visible light with a time interval of 30 minutes. After that 3 ml of the mixture was pipetted out and UV -VIS spectra was determined and absorbance was recorded. The photocatalyst was recovered by centrifugation following one full cycle of the experiment, and a recyclability test was run. Rhodamine B (RB) underwent a similar test, and the absorbance was also determined.

3. **Characterization:** The size and phases of the catalyst were determined using an X-ray diffractometer (Panalytical Model X' Pert Pro) operational with Cu-K radiation (λ=1.54 A^0). FESEM (Carl Zeiss, SMTAG) was used to study the morphology. To evaluate the energy band gap, UV-VIS spectrophotometer (M/s Shimazdu, UV 1700) were used Photocatalytic (PC) effectiveness was studies by taking phenol and Rhodamine B as model dye.

III. RESULT AND DISCUSSION

1. **X-ray Diffraction and Microscopic Studies:** The XRD analysis of the pure ZnO and SnO_2 samples demonstrates the polycrystalline character of the materials. ZnO has a hexagonal wurtzite phase with a space group of P63/mc, and SnO_2 has a tetragonal rutile phase with a space group of P42/mmm, according to the XRD data. The XRD peak positions patterns were indexed using the standard JCPDS cards for ZnO (file no. 36-1451) and SnO_2 (file no. 41-1445) [13–14, 41]. Zinc oxide (ZnO) has very fine and sharp XRD peaks, while tin oxide (SnO_2) has broader peaks with greater FWHM values. These differences suggest that ZnO and SnO_2 have high crystallinity (larger grain size) and low

crystallinity (lower grain size). The XRD patterns of the composite samples (Figure-1) solely display the two phases (ZnO and SnO_2) and do not display any additional impurity phases. The crystal size of the samples was calculated using the Scherrer formula, and we discovered that it was 21 nm for pure ZnO and 11 nm for pure SnO_2 [17]. Therefore, as the concentration of SnO_2 in the composite increases, the average grain size of ZnO increases and SnO_2 considerably decreases. As mentioned before, ZnO nanoparticles can prevent SnO_2 from forming, which reduces grain size [13]. However, we have seen an increase in this value as the concentration of SnO_2 in the composite has grown [12], indicating that SnO_2 has the capacity to stimulate the formation of zinc oxide. The relative strength of the ZnO diffraction peaks has increased in the XRD spectrum of the sample with a high SnO_2 concentration (ZS2). By using FESEM data, the surface morphology of the samples seen in Figure-2 is made visible. The composite samples show a significant change in form when compared to pure samples. The FESEM image of the ZS1 samples is displayed in Figure-2, where crystallites with different sizes and forms from the pristine samples are visible. This type of morphological alternation occurs in a composite due to a modification in the particle growth environment for both oxides present.

2. **Optical Absorption Studies:** The samples' optical absorbance spectra, which were measured between 300 and 700 nm, are displayed in Figure-3. In composite samples, the absorbance peaks of SnO_2 and ZnO are redshifted to 338 nm and 373 nm, respectively. The peak was observed at 339 nm for sample ZS1 and 343 nm for sample ZS2. Pure ZnO's absorbance spectrum has a clear, sharp peak that suggests the formation of monodispersed ZnO crystallites. The strength of this peak diminishes with the addition of tin oxide and changes in its concentration for the composite samples. We calculated each sample's band gap (E_{BG}) using the formula E_{BG} (eV) = hc/λ. Planck's constant (h), the speed of light in vacuum (c), and the wavelength of vacuum absorption (λ) are represented, correspondingly. Using the above formula, the band gaps of SnO_2 and ZnO are determined to be 3.61 eV and 3.30 eV, respectively. These values shift to 3.63 eV and 3.56 eV for ZS1 and ZS2, respectively. As a result, it should be mentioned that the composite heterostructures' band gaps are greater than those of ZnO and lower than those of pure SnO_2.

3. ***Photocatalytic Study:*** The effectiveness of photocatalysts in degrading pollutants like MB and Rhodamine B (RB) was evaluated in a photocatalytic study given in Figure 4. This was determined using the equation below:

$$\textit{Degradation Efficiency} = (1-C/C_0)\ X\ 100\% \quad \ldots\ldots\ldots\ldots\ldots\ldots\ (1)$$

Here, C represents the equilibrium dye solution concentration following UV-Vis light irradiation and C_0 represents the equilibrium dye solution concentration prior to UV-Vis light irradiation. To assess the chemical kinetics of the photocatalytic degradation of phenol and RB, the Langmuir-Hinshelwood (L-H) kinetic analysis (Eqn. 2) was modified [11,12].

$$r = \frac{dC}{dT} = \frac{kKC}{1+KC} \ldots\ldots\ldots\ldots\ (2)$$

The reactant oxidation rate (r) is expressed in mg/L min, the reactant concentration (C) is expressed in mg/L, the irradiation duration (t) is expressed in seconds, the reaction rate constant (k) is expressed in mg/L min, and the reactant adsorption coefficient (K) is expressed in L/mg. For the experiment, a low initial concentration was used, which caused the above equation to be simplified into a first-order equation (Eqn. 3).

$$Ln\frac{C}{C_0} = -kt \ldots\ldots\ldots\ldots\ldots (3)$$

The apparent first-order rate constant, k, is determined from the slope of the above line by linear regression, and the plot of Ln (C/C_0) over time results in a straight line Figure 5(a & b) depicts, in the presence of ZnO, SnO_2, ZS1 and ZS2 nanocatalysts, respectively, the change in phenol and RB concentration in the aqueous solution after sustained UV-Vis light exposure. Without the use of a catalyst, no discernible changes were seen in the concentration of phenol or RB. However, photon radiation and the use of a photocatalyst make it possible since the absorbance of phenol and RB falls substantially with photon radiation duration, which results in a noticeable increase in the photocatalytic efficiency. This aims to make contaminants degrade in visible light. The deterioration (%) under the influence of SnO_2 photocatalysts gradually rises with exposure time and reaches a maximum value of 80.45% in 180 minutes. Though, ZnO (a pure sample) has superior degrading efficiency than pure tin oxide. With a photocatalyst dosage of 15 mg/L, ZnO nanoparticles may simultaneously degrade phenol by up to 81.06%. The deterioration (%) in the composite heterostructure of ZnO and SnO_2, which was created by coupling the aforementioned two metal oxides, has increased further in comparison to both the pure samples. ZnO:SnO_2 photocatalysts (ZS1 sample) were able to degrade materials to about 89.11% of their initial state within 180 minutes of UV-Vis light irradiation time. The value of deterioration (%) for samples with a higher tin oxide content in the composite is lower than the figure above but is still higher than in the case of pristine samples.

According to a theory, phenol molecules undergo photocatalytic degradation and are changed into byproducts including benzoquinone, catechol, and hydro-quinone, which are then further oxidized to form mineral acids, CO_2, and water. These by-products overlap the degree of phenol degradation in the absorbance analysis because they are also absorbed in the same UV-Vis region as phenol. As a result, no notable modifications to the phenol absorption graph were seen for the photocatalytic degradation of phenol employing ZnO and SnO_2 nanoparticles [22]. However, when ZnO:SnO_2 was utilized as a photocatalyst, a significant result in terms of mineralization was obtained throughout the experiment. The degradation of RB was studied using a similar methodology, using the pure materials (ZnO & SnO_2) and nanocomposites as photocatalysts. The aforementioned investigation also revealed the degradation (%) of the color in question. For the SnO_2, ZnO, ZS1 and ZS2 samples, we found respective RB degradation rates of 78.23%, 82.41%, 84.5% and 83.2% (Figure-5b). For phenol and RB, respectively, the materials' estimated degradation efficiency (C/C_0) is depicted in Figure-5 (c & d). The rate of photodegradation is then followed by pseudo first order kinetics.

In this study, pseudo first order kinetic is followed for the photodegradation. The slope of the curve between $\ln(C_0/C_t)$ and irradiation time was used to calculate the rate constant (k), which is given in Table-1. The degradation of phenol and RB by the NCs has been found to have a greater rate constant (k) than the degradation of pure ZnO and SnO_2. As a result, when compared to the original samples (ZnO & SnO_2), the nanocomposites made by combining the aforementioned oxides can synergistically boost the photocatalytic activity. Of the two composite samples, ZS1 had a higher concentration of SnO_2 and a higher rate constant (k) value than ZS2 (Table-1). As a result, the previously described analysis has shown that the sample ZS5, the most effective photocatalyst for the photodegradation of phenol and RB, produces the highest level of degradation efficiency. In order to examine the impacts of photocatalyst loading, starting dye concentration, pH, and recyclability tests, ZS1 photocatalyst was found to be the most appropriate and effective composite photocatalyst. In order to form a heterostructure system during the photocatalytic process, SnO_2 is deposited onto ZnO. ZnO photocatalyst exposed to UV-Vis light promotes an electron from the valence band (VB) to the conduction band (CB). Now, this electron is in the CB of SnO_2 instead of the CB of ZnO. In this process, the electrons created by photons are sunk by the CB of SnO_2. Meanwhile, the opposite direction of migration of the photo-generated holes causes them to collect in the ZnO VB, improving the efficiency of charge separation. The photogenerated electrons and holes in ZnO:SnO_2 photocatalyst's surface promote the photocatalytic degradation of phenol and RB [14,16]. O_2 and H_2O are changed into the corresponding radicals O_2• and •OH by these recombination electro-hole pairs (e-h) [12,25]. Pollutant and dye molecules can be broken down by these radicals into intermediate chemicals, which can then go through the whole mineralization process (CO_2 + H_2O).

IV. CONCLUSION

The present study is aimed to investigate and differentiate the efficacy of a heterojunction nanocomposite (ZnO-SnO_2) in the effective photodegradation of organic dyes, specifically phenol and Rhodamine B, for environmental remediation purposes. The investigation of photocatalytic degradation in the context of two specific organic dyes demonstrates that the composite nanocatalysts have a greater effectiveness in degrading these dyes when compared to the individual oxides. The ZnO-SnO_2 binary heterojunction demonstrates enhanced efficiency in separating electron and hole pairs, thereby reducing carrier recombination and prolonging their lifetimes. This results in the generation of a greater number of OH• radicals, which play a crucial role in decomposing organic dyes.

REFERENCES

[1] A. Haleem, M. Javaid, R. P. Singh, S. Rab, R. Suman, Global Health Journal, 7 (2023) 70-77, https://doi.org/10.1016/j.glohj.2023.02.008.
[2] D. Sahu, N.R. Panda, B.S. Acharya, A.K. Panda, Optical Materials, 36 (2014) 1402-1407, http://dx.doi.org/10.1016/j.optmat.2014.03.041.
[3] D. Sahu, B.S. Acharya, A.K. Panda, Ultrasonics Sonochemistry, 18 (2011) 601-607, https://doi.org/10.1016/j.ultsonch.2010.08.012.
[4] D. Sahu, N.R. Panda, B.S. Acharya, A.K. Panda, Ceramics International, 40 (2014) 11041-11049, http://dx.doi.org/10.1016/j.ceramint.2014.03.119.
[5] D. Sahu, B.S. Acharya, B.P. Bag, T.B. Singh, R.K. Gartia, Journal of Luminescence, 130 (2010) 1371-1378, https://doi.org/10.1016/j.jlumin.2010.02.049.

[6] N.R. Panda, D. Sahu, B.S. Acharya, P. Nayak, Current Applied Physics, 15 (2015) 389-396, http://dx.doi.org/10.1016/j.cap.2015.01.014.
[7] D. Dash, N.R. Panda, D. Sahu, Applied Surface Science, 494 (2019) 666-674, https://doi.org/10.1016/j.apsusc.2019.07.089.
[8] D. Sahu, N.R. Panda, B.S. Acharya, Materials Research Express, 4 (2017) 114001, https://doi.org/10.1088/2053-1591/aa9597.
[9] N.R. Panda, D. Sahu, B.S. Acharya, Journal of nanoscience and nanotechnology, 12 (2012) 6977-6986, https://doi.org/10.1166/jnn.2012.6567.
[10] N.R. Panda, D. Sahu, S. Mohanty, B.S. Acharya, Journal of nanoscience and nanotechnology, 13 (2013) 427-433, https://doi.org/10.1166/jnn.2013.7073.
[11] N.R. Panda, D. Sahu, B.S. Acharya, P. Nayak, S.P. Pati, D. Das, Acta Metallurgica Sinica (English Letters), 27 (2014) 563-568, https://doi.org/10.1007/s40195-014-0093-8.
[12] D. Sahu, B.S. Acharya, N.R. Panda, AIP Conference Proceedings, 1728 (2016) 020165, https://doi.org/10.1063/1.4946216.
[13] D. Dash, N.R. Panda, D. Sahu, Nano Express, 2 (2021) 010007, https://doi.org/10.1088/2632-959X/abd90b.
[14] N.R. Panda, D. Sahu, Heliyon, 6 (2020) e04717, https://doi.org/10.1016/j.heliyon.2020.e04717.
[15] D. Sahu, Russian Journal of Chemistry, 93 (2020) 905-915, https://doi.org/10.1134/S107042722006018X.
[16] A. Palai, N.R. Panda, D. Sahu, Journal of Molecular Structure, 1244 (2021) 131245, https://doi.org/10.1016/j.molstruc.2021.131245.
[17] A. Palai, N. R. Panda, S. Chhotaray, and D. Sahu, Surfaces and Interfaces, 41 (2023) 103217, https://doi.org/10.1016/j.surfin.2023.103217.
[18] A. Palai, N. R. Panda, and D. Sahu, ECS J. Solid State Sci. Technol., 12 (2023) 076015, doi: 10.1149/2162-8777/ace84c
[19] D. Sahu, N.R. Panda, B.S. Acharya, A.K. Panda, AIP Conference Proceedings, 1591 (2014) 276, https://doi.org/10.1063/1.4872571.
[20] N.R. Panda, S.P. Pati, D. Sahu, D. Das, Materials Letters, 300 (2021) 130170, https://doi.org/10.1016/j.matlet.2021.130170.
[21] D. Sahu, N.R. Panda, Current Nanoscience, 17 (2021) 162-169, https://doi.org/10.2174/1573413716999200728175722.
[22] D. Sahu, A. Palai, N.R. Panda, Journal of Materials Science: Materials in Electronics, 33 (2022) 8504-8518, https://doi.org/10.1007/s10854-021-06401-8.
[23] P.K. Mishra, N.R. Panda, S.P. Pati, S.K. Biswal, D. Sahu, ECS Journal of Solid State Science and Technology, 10 (2021) 071006 (2021), https://doi.org/10.1149/2162-8777/ac0cc6.
[24] S. Dhal, P. Das, A. Patro, M. Swain, S.R. Hota, D. Sahu, S. Chatterjee, Radiation Physics and Chemistry, 188 (2021) 109649, https://doi.org/10.1016/j.radphyschem.2021.109649.
[25] D. Sahu, N.R. Panda, D. Dash, Asian Journal of Chemistry, 32 (2020) 1809-1814 (2020), https://doi.org/10.14233/ajchem.2020.22726.
[26] D. Sahu, N.R. Panda, B.S. Acharya, AIP Conference Proceedings, 1665 (2015) 050013 (2015), https://doi.org/10.1063/1.4917654.
[27] N.R. Panda, D. Sahu, B.S. Acharya, P. Nayak, AIP Conference Proceedings, 1665 (2015) 050027, https://doi.org/10.1063/1.4917668.
[28] N R Panda and B S Acharya, Materials Research Express, 2 (2015) 015011, DOI: 10.1088/2053-1591/2/1/01501.
[29] N.R. Panda, S.P. Pati, D. Das, Applied Surface Science, 491 (2019) 313-318, https://doi.org/10.1016/j.apsusc.2019.06.152.
[30] N. R. Panda, B.S. Acharya, P. Nayak, Nanoscience and Nanotechnology Letters, 4 (2012) 808-813, https://doi.org/10.1166/nnl.2012.1430.
[31] N.R. Panda, B.S. Acharya, P. Nayak, S.P. Pati, B.K. Nath, D. Das, Physica B: Condensed Matter, 407, 2716-2720 (2012), https://doi.org/10.1016/j.physb.2012.03.071.
[32] N.R. Panda, S.P. Pati, A. Das, D. Das, Applied Surface Science, 449 (2018) 654-659, https://doi.org/10.1016/j.apsusc.2017.12.003. N. R. Panda, B. S. Acharya and P. Nayak, Journal of Materials Science: Materials in Electronics, 24 (2013) 4043–4049, https://doi.org/10.1007/s10854-013-1359-z.
[33] N.R. Panda, B.S. Acharya, P. Nayak, Materials Letters, 100 (2013) 257-260, https://doi.org/10.1016/j.matlet.2013.03.059.

[34] N.R. Panda, B.S. Acharya, P. Nayak, B.P. Bag, Ultrasonics Sonochemistry, 21 (2014) 582-589, https://doi.org/10.1016/j.ultsonch.2013.08.007.
[35] N.R. Panda, B.S. Acharya, T. B. Singh, R.K. Gartia, Journal of Luminescence, 136 (2013) 369-377, https://doi.org/10.1016/j.jlumin.2012.12.002.
[36] S. Acharya, S.K. Biswal, S.N. Sarangi, Chemical Physics, 523 (2019) 99-105, https://doi.org/10.1016/j.chemphys.2019.04.014.
[37] D. Dash, D. Sahu, IOP Conference Series: Materials Science and Engineering, 1219 (2022) 012037, https://doi.org/10.1088/1757-899X/1219/1/012037
[38] A. Palai, N. R. Panda, M. R. Sahoo, and D. Sahu, Journal of Materials Science: Materials in Electronics, 33 (2022) 9599-9615, http://dx.doi.org/10.1007/s10854-021-07583-x
[39] D. Dash, A. Palai, D. Sahu, Ceramics International, 48 (2022) 28835-28842, https://doi.org/10.1016/j.ceramint.2022.03.139.
[40] M.T. Uddin, Y. Nicolas, C. Olivier, T. Toupance, L. Servant, M.M. Müller, H.J. Kleebe, J. Ziegler, and W. Jaegermann, Inorg. Chem., 51 (2012) 7764−7773. dx.doi.org/10.1021/ic300794j
[41] A. Mills, S.L. Hunte, J. Photochem. Photobiol. A Chem. 108(1) (1997) 1-35. https://doi.org/10.1016/S1010-6030(97)00118-4
[42] A. Hamrounia, N. Moussaa, F. Parrinob, A.D. Paolab, A. Houasa, L. Palmisano, J. Mol. Catal. A: Chem., 390 (2014) 133–141. http://dx.doi.org/10.1016/j.molcata.2014.03.018
[43] R. Lamba, A. Umar, S.K. Mehta, S.K. Kansal, J. Alloys Compd., 653 (2015) 327-333. http://dx.doi.org/10.1016/j.jallcom.2015.08.220
[44] A.M. Al-Hamdi, U. Rinner, M. Sillanpää, Process Safety and Environmental Protection., 107 (2017) 190–205. http://dx.doi.org/10.1016/j.psep.2017.01.022
[45] S.Y. Lee, S.J. Park, J. Ind. Eng. Chem., 19(6) (2013) 1761-1769. https://doi.org/10.1016/j.jiec.2013.07.012.

Table 1: Degradation (%) and rate constant estimated from the photocatalytic experiment after 180 min of light irradiation**.**

Sl. No	% of Degradation		Rate constant (k) min^{-1}	
	Phenol	Rhodamine B	Phenol	Rhodamine B
SnO_2	81.2	78.2	0.0112	0.0137
ZnO	80.45	82.41	0.0156	0.0141
ZS1	89.11	84.5	0.0391	0.0284
ZS2	83.45	83.2	0.0225	0.0271

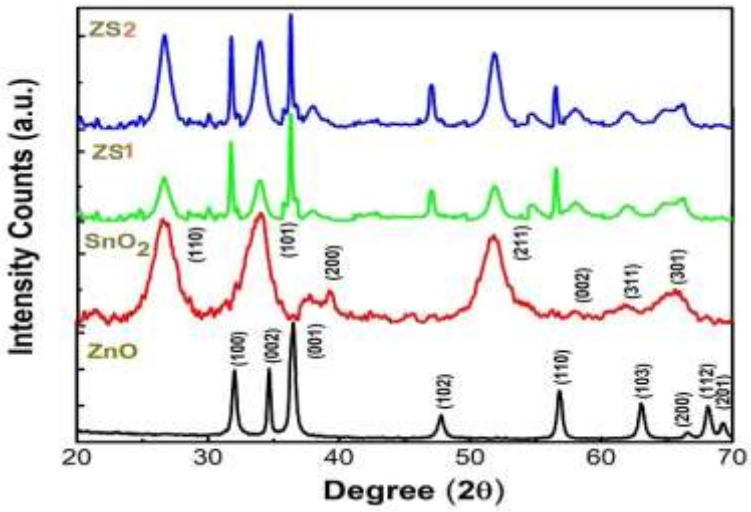

Figure 1: XRD patterns of ZnO, SnO_2, ZS1 and ZS2 nanocomposites.

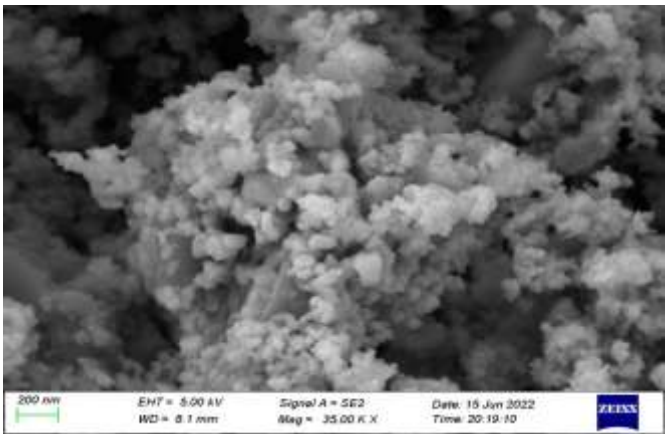

Figure 2: FESEM images of ZS1 nanocomposite.

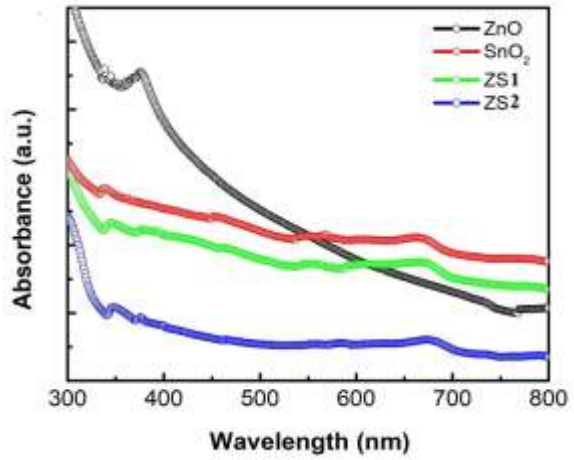

Figure 3: UV-Vis absorption spectra of ZS1 binary nanocomposites.

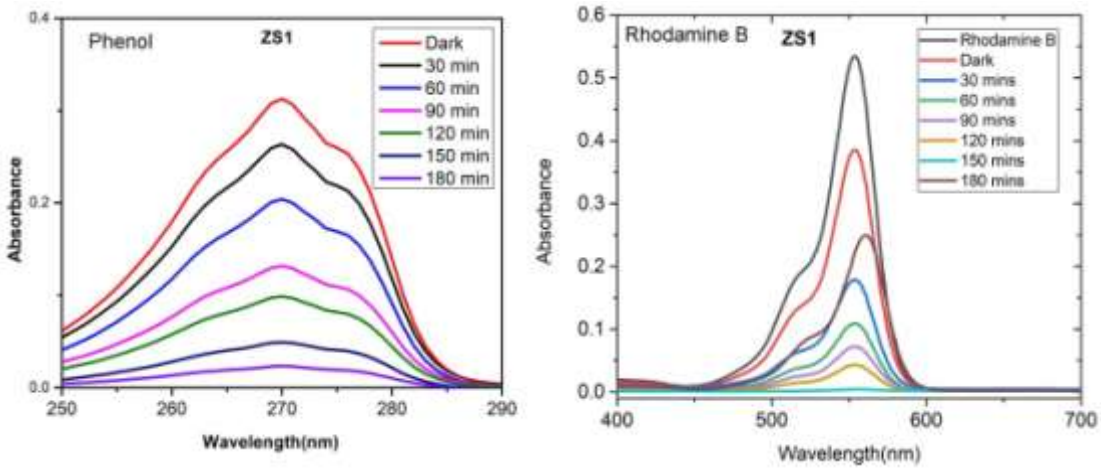

Figure 4: Absorption spectra of Phenol and Rhodamine B showing photodegradation by ZS1 binary Photocatalyst.

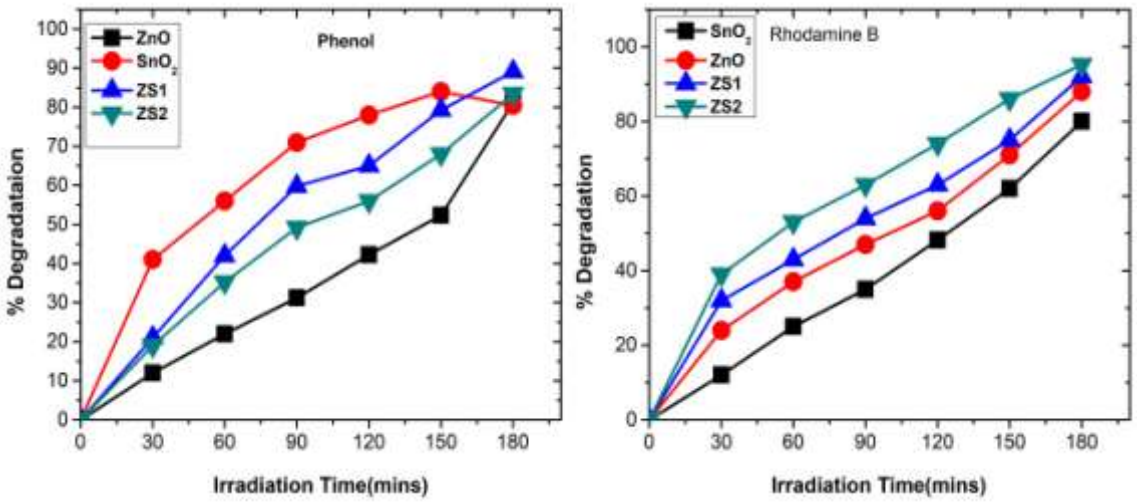

Figure 5: Photodegradation of phenol and RB with different photocatalysts.

